Complexity in electro-optic delay dynamics: modelling, design and applications

Laurent Larger

Complexity in electro-optic delay dynamics: modeling, design, and applications

Laurent Larger

FEMTO-ST Institute, UMR CNRS 6174, Optics Dept. P.M. Duffieux
University of Franche-Comté, 16 route de Gray, 25030 Besançon cedex, France

Nonlinear delay dynamics have found during the last 30 years a particularly prolific exploration area in the field of photonic systems. Besides the popular external cavity laser diode setups, we will focus in this article on another experimental realization involving electro-optic (EO) feedback loops, with delay. This approach has strongly evolved with the important technological progress made on broadband photonic and optoelectronic devices dedicated to high speed optical telecommunications. The complex dynamical systems performed by nonlinear delayed electro-optic feedback loop architectures, were designed and explored within a huge range of operating parameters. Thanks to the availability of high performance photonic devices, these electro-optic delay dynamics led also to many successful, efficient, and diverse applications, beyond the many fundamental questions raised from the observation of experimental behaviors. Their chaotic motion allowed for a physical layer encryption method to secure optical data, and this in real time at the typical speed of modern optical telecommunications. Microwave limit cycles generated in similar EO delay oscillators, showed significantly improved spectral purity thanks to the use of a very long fiber delay line. Last but not least, a novel brain inspired computational principle has been recently implemented physically in photonics for the first time, again on the basis of an EO delay dynamical system. In this latter emerging application, the computed result is obtained by a proper "Read-out" of the complex nonlinear transients emerging from a fixed point, the transient being issued by the injection of the information signal to be processed.

Key words: Nonlinear delay dynamics, electro-optic delay oscillators, chaos, microwave optoelectronic oscillators, photonic neuromorphic computing, reservoir computing.

1. Early electro-optic delay dynamics

The Lorenz Butterfly effect (also known in a more academic way as "sensitivity to initial conditions") is originating from a 1963 publication, and it strongly contributed to the important revival of nonlinear dynamics theory. This occurred many years after the interrupted path drawn by Poincaré in the late 19^{th} and early 20^{th} century. The field of nonlinear dynamics was later popularized by Yorke in the 70s, while renaming this field "chaos theory". Important efforts were then brought in this emerging scientific community to show evidence of chaotic motion in real world, whether in systems observable in the Nature, or in artificial ones designed by humans. In the particular field of Optics, a seminal idea was proposed in the late 70s by a japanese researcher, K. Ikeda, in order to observe chaotic motions

Proc. R. Soc. A 1–23; doi: 10.1098/rspa.00000000

in Optics, the dynamical variable being the light intensity at the output of a ring cavity containing a Kerr medium (see Fig. 1(left)) [15].
A rapid physical look at this "Gedanken" experiment immediately reveals the central role of the delay induced by the time of flight of the light propagating inside the ring cavity. A simple dynamical modeling of the system can lead to the reduction of the number of dynamical variables to a single one, the laser output intensity. In this setup, this light intensity level is also repsonsible for the optical phase variations induced by the Kerr effect, at a rate of change γ limited only by this ultra fast light-matter interaction phenomenon. One is then brought to a scalar linear first order differential equation, driven by a nonlinear feedback term delayed in time. If no delay were present, it is known to always lead to a fixed point as the most complex possible solution. Bistable fixed points are however possible even without delay, because of the nonlinear feedback term occurring inside the cavity at the input of the Kerr medium. This nonlinear transformation is performed by an interference phenomena occuring between the input CW laser beam, and the cavity feedback beam. The actual presence of the delay violently changes the dynamical perspectives on this simple system, increasing its number of degrees of freedom from 1 (the intensity at the time origine), to infinity. This delay-induced infinite number of degrees of freedom stems from the size of the initial conditions formed, when delay is present, by a functional decribing the actual intensity variations in time, over a duration corresponding to the delay time τ_D. This delay interval can then be viewed as the "memory" of the cavity. Again, a rapid physical analysis of the relative time scales, would easily convince anyone that this delay potentially induces a from far non negligeable "memory" effects on the dynamics: the rate of change γ for a Kerr effect is of the order of ps^{-1} or even $(sub\text{-}ps)^{-1}$ time scale, whereas the time of flight of the light in vacuum easily exceeds ns (3 orders of magnitude greater!) even when only a few cm cavity length is concerned. This makes a strong evidence of the importance of the large delay situation in which the setup has to be considered.
In such an Ikeda ring cavity, high complexity chaotic motions were indeed obtained numerically. This was also confirmed experimentally, but on a modified setup. This alternative setup was however still following the typical ingredients described above, a delayed feedback loop with a modulated interference condition. In [13], a bulk electro-optic birefringent interferometer was proposed instead of the optical cavity, and the delay was performed via a digital buffer after analogue-to-digital conversion of the photodetected interference intensity. After being transformed back to a continuous time signal by a digital-to-analogue converter and some amplification, this delayed electronic signal was finally used as the drive of the electro-optically induced phase shift in the interferometer. Instead of this bulk setup, an integrated optics version was proposed right after in [33]. This technological solution is the one concerned by most of the results reported in this article. It is indeed a very convenient experimental approach, both from the system integration perspectives, as well as from the ones of the setup stability and performances. As it will be shown in this article, the extremely robust and reliable features of the related off-the-shelf optical telecommunication devices, transformed the original Ikeda ring cavity into a flexible photonic lab tool for harnessing the complexity of delay dynamics.

2. Modeling and design

The Ikeda ring cavity dynamics principle, once translated into a signal processing approach, appears as an obvious feedback loop chain. One of its main advantage is to allow for a clear separation between the linear and the nonlinear contributions in the dynamics. These issues will be detailed and analysed in the following subsections.

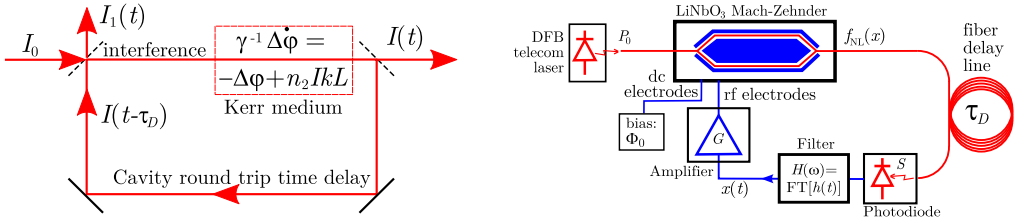

Figure 1. Ikeda dynamics: from the "Gedanken" experiment to the electro-optic implementation. Left: The Ikeda ring cavity ingredients: a nonlinear modulation of the intensity is performed via an interference condition modulated by the phase shift $\Delta\varphi$ occurred at one round trip earlier in a Kerr medium (length L, Kerr coefficient n_2). The input laser beam has a constant intensity I_0 and a wave vector $k = 2\pi/\lambda = 2\pi\nu/c$ in vacuum. The dynamics of the phase shift is ruled by the Kerr response time $\tau = \gamma^{-1}$. The dynamics can be observed through the intensity fluctuations at any output of the two partially reflecting mirrors of the cavity. Right: The intensity electro-optic nonlinear delay oscillator: a laser diode is seeding an electro-optic Mach-Zehnder (MZ) modulator with a continuous wave light beam of power P_0; the MZ output interference is (i) dynamically modulated by the electrical input $G\,x(t)$, and (ii) statically set by the offset phase Φ_0 (set by a constant voltage on the dc electrode); the resulting nonlinear transformation $f_{\mathrm{NL}}(x)$ is delayed in time by τ_D (flight time through a fiber); the modulated and delayed optical intensity is detected by a photodiode (sensitivity S); the resulting electrical signal is filtered in the Fourier domain according to $H(\omega)$, and amplified (gain G), then serving as the rf input of the MZ.

(a) *Modeling: a signal processing approach*

The simplified physical equation as written in the Kerr medium box of Fig.1(left), can be re-written with a splitting of the linear terms in the left hand side, and the nonlinear term in the right hand side. One can then analyse the dynamics as follows: in the time domain, it consists of a linear first order differential process driven by a nonlinear delayed feedback term; in the Fourier domain, the left hand side plays the role of a linear first order filter (actually a low pass filter) driven at its input by a delayed nonlinear transformation of its output. This results from a straightforward calculation as described in Eq.(2.1), using conversion rules between the Fourier and the Time domain (according to Fourier Transformations (FT), $\mathrm{d}/\mathrm{d}t \to i\omega\cdot\mathrm{FT}$, and $\int \mathrm{d}t \to (i\omega)^{-1}\cdot\mathrm{FT}$):

$$\tau\frac{\mathrm{d}\delta\varphi}{\mathrm{d}t}(t) + \delta\varphi(t) = f[\delta\varphi(t-\tau_D)] = z(t) \quad \xrightarrow{\mathrm{FT}} \quad \frac{\Delta\varphi(\omega)}{Z(\omega)} = \frac{1}{1+i\omega\tau} = H(\omega), \tag{2.1}$$

where $Z(\omega) = \mathrm{FT}[z(t)]$ and $\Delta\varphi(\omega) = \mathrm{FT}[\delta\varphi(t)]$ are the Fourier Transforms of the corresponding time variations. The Fourier Transform $H(\omega)$ represents the linear

filtering performed on the input signal and thus leading to the output signal. This filter is actually involved in the feedback loop architecture, i.e. it is the first order low pass filter in the particular case of Eq.(2.1). It is typically characterised by a -3 dB cut-off frequency of $(2\pi\tau)^{-1} = \gamma/(2\pi)$. One could notice that any other filter could be in principle considered with the same modeling approach. This results in a change of the Fourier filtering function $H(\omega)$, according to the actual filter to be considered. The consequence in the time domain would consist in the presence of higher order differential terms, as well as also eventually in additional integral terms. One might recall that $H(\omega)$ is defined as FT$[h(t)]$, where $h(t)$ is the so-called temporal impulse response of the corresponding linear filter, i.e. the filter output signal when the input is a Dirac function $\delta(t)$. With this modeling approach allowing for different kinds of filters, the right hand side of the differential equation remains unchanged, since it consists in the nonlinear delayed feedback driving the input of the linear filter. In our particular experimental scheme, the nonlinear transformation is ruled by a two-wave interference phenomena, i.e. $z(t) = A[1 + B\cos[\delta\varphi(t - \tau_D) + \Phi_0]\}$. A and B are constant parameters defined by the feedback gain, and the contrast of the intereference respectively. $B = 1$ for a unity contrast, i.e. when balanced wave amplitudes are concerned in the interference, and $A \propto n_2 k I_0/2$, as illustrated in Fig.1(left).
In practical situations where broadband or high frequency delayed optoelectronic feedback is involved, the low pass filtering has typically to be replaced by a bandpass filter to reflect the actual filtering performed by the electronic branch of the loop. In such a situation, the most simple linear filter model corresponding to a bandpass filtering, is a two pole (second order) Fourier transfer function $H(\omega)$. More physically and "time domain" speaking, this filtering situation is the one obtained in a damped oscillator, with the well known differential model of the following form:

$$H(\omega) = \frac{i2m\,\omega/\omega_0}{1 + i2m\,\omega/\omega_0 - (\omega/\omega_0)^2}, \quad \stackrel{\mathrm{FT}^{-1}}{\longrightarrow} \tag{2.2}$$

$$\frac{\omega_0}{2m}\int \delta\varphi\,\mathrm{d}t + \delta\varphi + \frac{1}{2m\omega_0}\,\dot{\delta\varphi} = z \quad \Leftrightarrow \quad \delta\varphi + \frac{2m}{\omega_0}\,\dot{\delta\varphi} + \frac{1}{\omega_0^2}\,\ddot{\delta\varphi} = \frac{2m}{\omega_0}\,\dot{z}$$

where $\dot{x}$ is the derivative of x with respect to time, m is the damping factor, and $2\pi/\omega_0$ the pseudo oscillation period. In this case of a second order bandpass filter, the discussion with respect to the damped oscillator analogy typically involves the nature of the eigenvalues. On the one hand, one can have complex eigenvalues when $m \ll 1$, in the case of a weakly damped oscillator and thus a narrow filtering around a central resonance frequency ω_0. This is the typical situations met in high spectral purity delay optoelectronic microwave oscillators ($\omega_0/(2\pi) \simeq 10$ GHz, and -3 dB bandwidth $m\omega_0 \simeq 10$s MHz), as proposed in [43]. On the other hand, the eigenvalues can be purely real and negative, which is met in a strongly damped oscillator with $m \gg 1$, ω_0 being then the geometric mean of the caracteristic cut-off pulsation $\sqrt{\omega_h\omega_l}$. In this case, the filtering features are as follows: (i) a -3 dB high cut-off frequency $\omega_h/(2\pi) = f_h \simeq 10$ GHz is corresponding to a low pass filter as in Eq.(2.1) with $\tau = \omega_h^{-1} = (2m\,\omega_0)^{-1} \simeq 10$ ps; (ii) and a low cut-off frequency $\omega_l/(2\pi) = f_l \simeq 10$s kHz corresponding to a high pass filter, and introducing a slow integration characteristic time as in Eq.(2.2) $\theta = \omega_l^{-1} = 2m/\omega_0$ of a few μs.

The case of negative real eigenvalues characterises the situation typically met in broadband optoelectronic chaos communication applications, as proposed in [14, 22, 3]). The modified Ikeda dynamics from (2.1) into (2.2) has been named integro-differential nonlinear delay equation, since it is written as follows in a normalized amplitude form, keeping the same $\cos^2$ nonlinear delayed feedback term in the right hand side:

$$\begin{aligned} \frac{1}{\theta}\int_{t_0}^{t} x(\xi)\,\mathrm{d}\xi + x(t) + \tau\frac{\mathrm{d}x}{\mathrm{d}t}(t) &= f_{\mathrm{NL}}[x(t-\tau_D)] - f_{\mathrm{NL}}[0] \\ &= \beta\cdot\{\cos^2[x(t-\tau_D)+\Phi_0] - \cos^2\Phi_0\}, \end{aligned} \tag{2.3}$$

where β is the normalised weight of the nonlinear function f_{NL} in the dynamics, and Φ_0 is a static phase shift defining the interference condition around which the dynamical modulation of the MZ occurs. The normalised dynamical variable $x(t)$ is determined so that it appears as a scale free argument of the $\cos^2$ nonlinear function. It is physically proportional to the original Kerr phase shift $\delta\varphi$ in the Ikeda model, or in the MZ case, it is proportionnal whether to the electro-optically induced phase shift or also to the rf voltage driving the MZ. One would notice that a constant term was added to the right hand side ($f_{\mathrm{NL}}[0]$) only for convenience, because this writing allows to highlight the fact that $x\equiv 0$ is a natural steady state in integro-differential delay dynamics. The model in Eq.(2.3), eventually with minor modifications depending on particular experimental conditions, was successfully used to investigate whether numerically or analytically many specific dynamical motions observed with the bandpass version of the generic electro-optic intensity setup (see Fig.1(right), [17, 8, 36, 6, 32]). It is sometimes more convenient to re-write the dynamics in a vectorial form, with a time $s=t/\tau_D$ normalized to the delay. The equations of motion read then as follows:

$$\begin{aligned} \varepsilon\cdot\dot{x}(s) &= -x(s) - \delta\cdot y(s) + f_{\mathrm{NL}}[x(s-1)] - f_{\mathrm{NL}}[0], \\ \dot{y}(s) &= x(s). \end{aligned} \tag{2.4}$$

The previous formulation of the dynamics might be particularly usefull in the broadband case, in order to highlight a few parameters revealing the important underlying multiple time scales problem: $\varepsilon=\tau/\tau_D \ll 1$ and $\delta=\tau_D/\theta \ll 1$ as in [36, 42], where the various relevant time scales are spanned over more than 6 orders of magnitudes.
The actual dynamical features which can be reached experimentally, strongly depend on the devices and system organisation. To clarify this from the practical point of view, we will address a few experimental details in the next subsection, trying to connect the technical characteristics of the devices used to build the electro-optic delay oscillator, together with some expected dynamical features.

(*b*) *Device features, and delay system properties*

In this subsection, many numerical values for the experimentally achievable parameter range will be given and discussed in the context of the dynamical properties of the electro-optic delay dynamics. Each of the devices depicted in the setup of Fig.1(right) will be addressed.

(b.1) *Amplitude parameters*

As indicated in Eq.(2.3), essentially two independent amplitude parameters can be defined for the characterization of the nonlinear function: (i) β is a weight for $f_{\rm NL}[x]$, acting as a vertical stretching in the graph of $f_{\rm NL}$); (ii) Φ_0 is an offset phase defining the mean operating point, it is acting as an horizontal shift in the graph of $f_{\rm NL}$ (see Fig.2).
The physical origine defining $\beta = \pi SGP_0/(2V_{\pi_{\rm rf}})$ comes from the various amplification factors and conversion efficiencies of each device in the feedback loop. The most important device is the electro-optic Mach-Zehnder (MZ) modulator performing the nonlinear transformation in the dynamics, a $\cos^2$-transformation. It is practically obtained from an electro-optically tuneable integrated optics two wave interferometer. The constructive interference are leading to the maximum of the function $f_{\rm NL}$ (plotted in Fig.2 Left), and the destructive one correspond to the minima of the function. With an EO Mach-Zehnder device, the interference condition can be dynamically controlled over a large bandwidth, i.e. the one typically involved in optical telecommunication systems for which they are commonly designed and used. The electro-optic efficiency is quantified technically by the half wave voltage $V_{\pi_{\rm rf}}$. It corresponds to the input voltage amplitude required to induce a π-phase shift in the interference condition, thus changing for example a constructive interference into a destructive one. The voltage amplitude ΔV applied to the MZ electrodes, when rescaled with respect to $V_{\pi_{\rm rf}}$, can be viewed as a measure of the nonlinear strength actually involved in the dynamics. More mathematically speaking, $(1 + \Delta V/V_{\pi_{\rm rf}})$ is an estimate of the equivalent degree for the polynomial that could approximate the actually used range of the nonlinear function. This would be for example a parabola when $\Delta V \simeq V_{\pi_{\rm rf}}$, or a cubic polynomial when $\Delta V \simeq 2V_{\pi_{\rm rf}}$, etc.... Highly nonlinear motions are thus subject to the capability to provide a voltage large enough compared to $V_{\pi_{\rm rf}}$, over the full bandwidth of interest (> 10 GHz for telecom devices). Currently, the most efficient Telecom MZ have a $V_{\pi_{\rm rf}}$ of about 3 Volts, but common values are usually closer to 5 Volts. The technical challenge becomes then obvious, for a cubic motion one would need to drive the MZ with ca. 15 Volts, which is commonly slightly above the limits of conventional MZ telecom drivers. Higher voltage spans are however possible, but usually at the cost of a strongly reduced bandwidth. A proper signal amplification is thus required, which is the role of the optoelectronic feedback. It is intended to provide enough detection efficiency and amplification, up to the requested drive voltage amplitude to be applied to the MZ. When broadband operation is desired, this implies a 50 Ω termination at the MZ electrodes, which is imposing an additional technical constrain in terms of rf power drive capability (up to a few electrical Watts). Assuming one has a standard "telecom" maximum optical power available at the photodiode input (fluctuations from 0 to 10 mW), and taking into account the typical detection efficiency of 0.9 A/W for InGaAs telecom photodiodes loaded with 50 Ω transimpedance amplifier, the electronic gain required from the photodiode to the driver, rises to a few 30 dB when quadratic nonlinear operation is expected. Neverheless, broadband amplified photodiodes are commercially available with up to 2.4 kΩ transimpedance instead of the previous 50 Ω. This is relaxing the remaining electrical gain to less than 20 dB. Though this consists already in a strong amplification, especially for bandwidth greater than 10 GHz,

it is technically feasible. When amplifier drive saturation is experienced, one could modify the model in Eq.(2.3) with an additional nonlinear transformation, a $\tanh(x)$ as the argument of the $\cos^2$ main non linearity instead of x (see [17, 6]). The progress in novel photonic technologies (plasmonic and/or photonic crystal devices) might further improve the actually achievable range for the nonlinear operation of electro-optic nonlinear delay oscillators. This corresponds to the design capability of devices with lower half wave voltage. Alternative setups and physical solutions can be found in the literature, however usually at the cost of strongly reduced bandwidth. This is for example the case for the wavelength chaos generator reported in [21, 31], where a polynomial up to 14th degree can be achieved due to the large, but slow, tuning range of a tunable DBR semiconductor laser. The achievable wavelength deviation can drive up to several free spectral range of a strongly imbalanced birefringent interferometer.
The parameter $\Phi_0 = \pi V_{\text{bias}}/(2V_{\pi_{\text{dc}}})$ is usually tunable over a large enough range, considering its π-periodicity in the model. As indicated in Fig.1(right), this parameter is simply adjusted via a constant voltage applied to the dc electrode of the MZ. This allows to adjust the operating point over more than one period of the $\cos^2$ modulation transfer function. With a $V_{\pi_{\text{dc}}}$ of about 4 to 7 Volts, with a purely capacitive load impedance and only very low frequency operation requirements, the only practical issue to check is the possible slow and small drift with external environment changes. Slow time scale relaxation phenomena, e.g. very slow dynamics induced by possible surface charge redistribution inside the electro-optic crystal, might occur, thus inducing a slow time dependence of the actual electro-optic efficiency.

(b.2) *Time parameters*

The key condition typically required when high complexity dynamics is desired, is the so-called large delay configuration. In that case, the delay τ_D is typically much greater than the characteristic time τ. The linear "memory" of the dynamics is thus scaled as the ratio τ_D/τ. This ratio can be viewed as simply representing the number of times that the fastest temporal motif limited by τ can be accumulated over a time interval corresponding to the delay τ_D. Complexity can be further increased through nonlinear effects: it was shown in [27, 28] that the attractor dimension of the Ikeda dynamics in chaotic regimes increases as $\beta\tau_D/\tau$.
From the more practical point of view, the setting of the time parameters depends on the targeted issues. For fundamental investigations of the dynamical properties of delay system, any setting can be adopted, depending on the studied configuration: accurately controlable and variable time parameters usually involves discrete time ([21]) or analogue-to-digital conversion ([10, 37, 38, 31]). The delay function is emulated by so-called FIFO (fist in first out) memories in the digital processing. The delay value is then fixed by the FIFO memory depth, and the digital clock defining the speed at which the samples are travelling through the FIFO. The delay value can be easily adjusted when tuning the digital clock frequency. When the FIFO is implemented in programmable digital devices (such as FPGA), even the linear filter can be implemented digitally, thus also providing a large flexibility, stability, and accuracy, in the definition of the filter properties. One has however to respect the basic rules of sampling theory (Shannon sampling

theorem), which is imposing limitations in terms of available analogue bandwidth depending on the maximum sampling rate. One has also to be aware of some signal to noise ratio limitations depending on the level of quantization. The digital approach has many advantages for more flexibility and robustness of the experimentally explored complex phenomena. Typical values of the ratio τ_D/τ is of the order of a few 10s, and the reference time scale τ is of the order of one or a few 10s of μs, resulting in delays of the order of ms.
When high speed is targeted, the natural choice is to perform the delay via the ultra broadband (10s THz) capacity of optical fibers. Optical fibers have also the attractive property to provide an ultra low absorption (typ. 0.2 dB/km) of the travelling light beam at the telecom wavelength (1.5 μm). This solution however leads to fixed delays, which value is directly determined by the length of the fiber. For example, a 4 km standard telecom grade single mode fiber spool provides ca. 20 μs delay, with an attenuation of less than 1 dB. The other time scales ruling the dfferential dynamics through the electronic filtering feedback, can be set to very fast dynamics when Telecom grade devices are used. Optoelectronic, electro-optic, and electronic devices can provide access to characteristic response time as fast as 10 ps. These devices are typically designed for communication bandwidth greater than 10 GHz. The large delay configuration is then easily fullfilled with a setup as in Fig.1(right), since only a few meters of fiber is generating 10 ns time delay, thus performing a normalised linear memory greater than 1000. Considering the fiber pigtails of commercial devices, 10s ns delays are simply obtained without any additional fiber spool. The memory of the delay can be increased by 3 additional orders of magnitude (1 million size linear "memory") when commercial fiber spool of several 10s of km are used. Within this extreme situation, subtil dispersion phenomena might have to be further considered in the dynamics, since ultra-fast dynamics leads to continuously spread time delays depending on the Fourier frequency components, as described in [25].

(*c*) *Dynamical and architectural diversity*

(c.1) *A few bifurcation issues*

A basic and common interpretation of delay differential equations (DDE, as in Eq.(2.1)) is usually done as a first approach for the understanding of some of its numerous behavior. It is typically called the adiabatic approximation, or the singular limit map, which consists in taking the limit $\varepsilon = \tau/\tau_D \to 0$. Under this asumption, the dynamics is reduced to a map $x_{n+1} = f[x_n] = \beta \cos^2[x + \Phi_0]$. The fixed points $x_{\mathrm{F}}(\beta, \Phi_0)$ are obtained from the transcendental equation $x_{\mathrm{F}} = f[x_{\mathrm{F}}]$, and they are the same for the DDE model. Graphically, these fixed points are found as the intersections between the graph of $y = f_{\mathrm{NL}}[x]$, and the first bissector $y = x$. There exists at least one solution between 0 and the normalized weight β, due to the bounded character of the two-wave intensity interference function. The number of intersections is increasing linearly with β. The stability of these fixed points under the map approximation, can be straightforwardly derived. It is ruled by the absolute value of the slope of the nonlinear function, evaluated at the fixed point, $|\beta \sin[2(x_{\mathrm{F}} + \Phi_0)]|$: it is stable if the value is smaller than 1, and unstable otherwise (see Fig.2). As a consequence, it is usually always possible to find one stable fixed points in the (β, Φ_0)-plane, if one selects Φ_0 such that the fixed point is close enough to an extremum of $f(x)$ (i.e. close to a constructive or

destructive interference). Conversely, since this value is proportional to the weight β, the stable fixed point can always be destabilized by increasing the feedback gain β, except for the exact constructive or destructive interference condition. Practical parameter values accessible experimentally, are covering easily the full π-periodicity range for Φ_0. However for β, it is usually limited to a few units (typ. $\simeq 5$) in the case of an electro-optic setup as in Fig.1(right).

Bifurcations and route to chaos are typically explored as the feedback gain β is

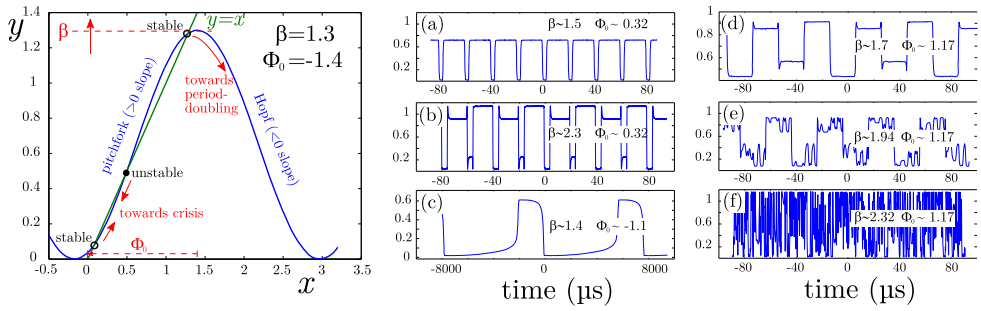

Figure 2. Route to chaos in delay dynamics. Left: graph of the Ikeda map $x_{n+1} = \beta \cos^2(x_n + \Phi_0)$, in which the pitchfork case is represented along the positive slope of the map model, leading to whether a period doubling or a crisis and a period doubling (see also Fig.3 for bifurcation diagrams). Center: unusual experimental time traces obtained with an integro differential ($\varepsilon \approx 0.015$ and $\delta \approx 0.628$) delay dynamics along the positive slope (up: τ_D-periodic limit cycle connecting the two stable fixed of the pitchfork map, with asymmetric duty cycle; middle: period doubled of the previous regime; low: slow θ-periodic limit cycle); theses regimes are only obtained with the integro-differential model, the upper and lower ones being bistable (hysteresis loop is obtained with respect to Φ_0, for the same β). Right: common regimes of the period doubling cascade, along the negative slope (up: period 4 limit cycle; middle: period-2 chaos; low: fully develop chaos).

increased. This is experimentally convenient since β can be directly and linearly tuned by the input optical power level P_0 as in Fig.1(right)). Under the map model, this route to chaos can be roughly divided into 2 scenarii depending on the sign of the slope around the original stable fixed point x_F (for small βs and depending on Φ_0).

- If the slope is positive, a pitchfork bifurcation occurs, leading to the appearence of two stable fixed points (with also positive slopes) separated by an unstable fixed point (see Fig.2): the dynamics exhibits bistability, the actually observed stable fixed point depends on the initial condition. The upper fixed point is the closest to a maximum of $f(x)$, i.e. to a constructive interference. As β is increased, it slides upward along f_{NL}, going through the constructive interference state, and then reaching the negative slope region. Further bifurcation of this stable fixed point along a negative slope region, is qualitatively the same as the one experienced by a stable fixed point originally located along the negative slope. If the actual intial fixed point if the lower one, it is the closest to the minimum of $f(x)$, i.e. to the destructive interference. On the contrary to the upper fixed point, it experiences a tangent bifurcation through a collision with the unstable fixed point when β is increased. Both fixed points then disappear after the bifurcation, leading to a crisis of the dynamics, with a jump onto the remaining fixed point

located close to the maximum of $f(x)$. The observed dynamics is then the one resulting from the bifurcation sequence experienced by the same fixed point from its stable steady state around a maximum of $f(x)$. If the parameter β is then decreased, the hysteresis cycle around the crisis point can be visited, highlighting the characteristic bistability around this point (see Fig.3).
In the case of a DDE model, novel solutions arises (see Fig.2-center and -right) with respect to the above described map model situation (Fig.2-left). A recently observed and analyzed one concerns a τ_D-periodic motion connecting plateaus. The values of the plateaus do not correspond to the common limit cycle of the map with a period of twice the delay, but they are corresponding to each of the two stable fixed points in Fig.2. Whereas such a solution was proven to be unstable or metastable for standard DDE with low pass feedback filter, the bandpass feedback was recently found to lead to a stable version of this particular τ_D-periodic solution [41, 40].
- If the slope is negative, the bifurcation scenario is very similar to the well known period doubling cascade route to chaos, popularized in the literature by the logistic map. The nonlinear function around a maximum of intereference is indeed locally a concave parabola, exactly as for the logistic map. In the real world of DDEs however, only the beginning of the period doubling cascade is observed up to period 8 or 16, depending on the noise level in the experiment. The amplitude separation in the limit cycle is smaller and smaller as the period doubling increases: when this separation is smaller than the noise experiment, they can not be distinguished. The limit cycles of the DDE take the form of alternating plateaus of duration corresponding to the delay τ_D. The amplitudes of the plateaus are matching the ones calculated for the map. The transitions between the successive plateaus are however not instantaneous as in the map, but they occur with ε-small transition layers. These layers are thus scaled in time with the response time τ, or equivalently, they are scaled with the inverse of the bandwidth limiting the feedback filtering. These jumps are also characterised by stronger and stronger overshoots or weakly damped oscillations, which are underlining the increasing role of the continuous time dynamics in the global solution. After what is called the accumulation point for the map (value of β leading to an infinite period limit cycle in 2^n as $n \to \infty$), a reverse period doubling cascade is observed (n now decreasing with increasing β). The accumulation point in β is located at the position of the vertical dashed line in Fig.3. A characteristic dynamics in this reverse cascade is qualitatively characterised by 2^n plateaus consisting of small chaotic fluctuations with amplitudes $\beta/2^n$ and with ε-small time scales, each plateau being separated by $2^n - 1$ forbidden amplitude bandgaps. As β passes the fully developed chaos limit found for the map (for which $n = 0$, i.e. when the full interval $[0, \beta]$ is densely visited by the corresponding dynamics), the actually observed dynamics are strongly dominated by the numerous continuous time modes of DDEs, which are corresponding to the large amplitude and high frequencies eigenmodes of the DDE characteristic equation: $1 + \varepsilon\lambda = f'(x_{\mathrm{F}})e^{-\lambda}$. Within this β-range, many qualitative features of the observed dynamics can be used to illustrate the much stronger influence of the continuous time dynamics compared to the discrete time map approximation. The high complexity regimes are thus strongly differing from the map situation (compare left and right diagrams for high β in Figs.3): (i)the amplitude probability density distribution becomes very smooth (whereas it is

discontinuous for the map); (*ii*)instead of the periodicity windows of the map, one can observe so-called higher harmonic synchronisation [16] revealing complex resonances with rational numbers between the short time scale τ, and the large delay τ_D; the chaotic attractor, instead of being included in a 1D phase space, reaches dimensions of the order of $\beta\tau_D/\tau$. In actual experiments, the chaotic attractor dimensions can easily reach more than several hundreds up to several thousands.

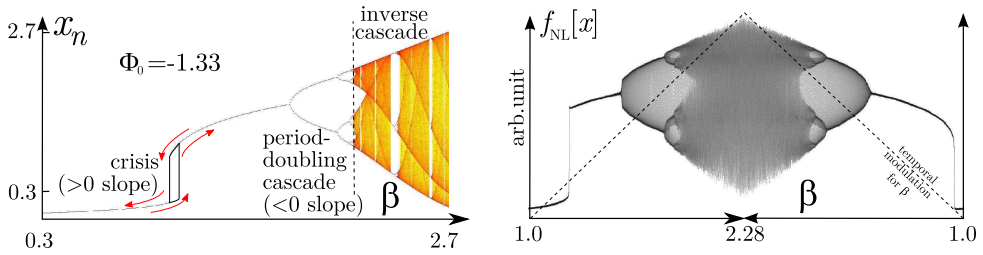

Figure 3. Bifurcation diagrams. Left: for the Ikeda map (numerics). Many values of the asymptotic solutions are calculated for each of the 800 β-values along the horizontal axis. The values are used to calculate a probability density function (PDF) for each β. The PDF is color encoded. Right: for the continuous time Ikeda model (experimental, low pass filter as in Eq.(2.1)). The bifurcation parameter β was slowly scanned with a triangular signal controlling the optical power seeding the MZ of the setup in Fig.1 Right. This allowed to increase and then decrease β in time, very slowly (0.5 s) compared to the characteristic time scales of the dynamics. Many points (10^7) are collected all along the scan, thus allowing to calculate an approached PDF with 10^4 values at each of the 1024 horizontal positions for β. The PDF is encoded in grey scale. Φ_0 is adjusted to a comparable value with respect to the left bifurcation diagram. Notice that solutions represented in Fig.2 Center are typical of the nonlinear delay integro-differential model, and can not be observed with the map, or the delay differential model of this figure. The solutions of Fig.2 Right are common to each of the dynamical models.

(c.2) *Setup design variations: even more motion complexity*

Though the initial Ikeda DDE model already features rich and highly complex dynamics, the experimental investigation of such systems largely contributed to the emergence of even reacher dynamics. New experiments performing EO delay dynamics in the framework of several practical applications, gave rise to various modeling modifications (see the sections below). This is typically one of the historical reason motivating fundamental studies on the integro-differencial nonlinear delay dynamics described in Eq.(2.3) or (2.4) instead of the DDE in Eq.(2.1). The presence of the integral term was originating from the design of broadband chaos generators for high speed optical chaos communications. In the case of such a wide bandwidth spanning over 6 orders of magnitude in the Fourier domain, from a few 10s of kHz to more than 10 GHz, it is technologically too difficult to have a DC preserving feedback. The broadband rf electronic amplifier of concern behave necessarily as bandpass filters. Such a situation required the introduction of an additional slow time scale θ attached to the low cut-off frequency of a few 10s of kHz. This led to a not yet exhaustive "zoology" of many new dynamics, such as chaotic breathers [20], slow limit cycle, pulsating regime

[36], novel crisis transisition from fixed point to chaos [6], τ_D-periodic limit cycle along the positive slope [41], Neimark-Sacker (torus) bifurcation of the limit cycle in very weakly damped ($m \ll 1$) microwave delay oscillators [8], etc....
Among other technological modifications of the original Ikeda dynamics, novel electro-optic architectures also led to a surprising modeling of this dynamics back to a map, however preserving the high-dimensional feature of the solutions [23]. Compared to the setup in Fig.1(right), the modification leading here to a correct map modeling is related to the use of a high repetition rate (>GHz) mode locked pulsed laser source. The condition leading to a map model is related to the fast optoelectronic devices capable to resolve the nonlinear feedback of the pulses within a time shorter than the repetition period of the laser. Dimensionality of the solutions is then ruled by the number of independent pulses stored in the feedback delay line, each pulse being ruled by the nonlinear map.
Other experimental investigations dedicated to optical chaos communication [29, 26, 25] proposed the introduction of a multiple delay electro-optic architecture. The specific device introducing a supplementary delay was a passive imbalanced DPSK (difference phase shift keing) demodulator. This led to the design of a 4 time scales delay dynamics, an additional short delay $\delta\tau_D$ being present due to the imbalance interferometer. Novel bifurcation phenomena of the first Hopf bifurcation were discovered in such a system, revealing a resonance condition between the small delay $\delta\tau_D$ and the large delay τ_D [42]. The bifurcation consists in the destabilization of the Hopf limit cycle ruled by the small delay, and the occurrence of a stable amplitude modulation of the Hopf cycle, with an envelope period ruled by the large delay.
Last but not least, in the framework of the investigation of a novel computational principle referred to as "Reservoir Computing" and based on the computational power provided by complex transient motion of high-dimensional dynamical system, a many delayed feedback (15 to 150 randomly distributed delays) dynamics was explored. Their motivation was related to the investigation of the connectivity enhancement of the equivalent virtual network of nodes, due to the multiple delayed feedback architecture [31]. The actual properties and features of this novel kind of complex multiple delay dynamics is still under investigations.

3. Delay dynamics meet applications

In the remaining sections, we will focus more on a few practical applications that were explored in the recent past years, specifically on the basis of various electro-optic nonlinear delay dynamics. We will connect the specific dynamical properties of the electro-optic delay oscillators of concern, to the actual physical requirements expected for each of these applications. The sequence of the three proposed applications will moreover scan a bifurcation diagram in the reverse direction: first, optical chaos communications will show how one can make use of the high complexity chaotic regimes to perform data encryption; second, the limit cycle of an optoelectronic microwave oscillator will benefit from high spectral purity provided by a long delay; and last, even the stable fixed point will be usefull as a stable starting point from which a complex transient is generated. This nonlinear transient dynamics is the complex response of the dynamics to an external signal encoding a problem to be solved. The nonlinear transient is

the conceptual basis for a novel universal computing principle exploiting high dimensional phase space of complex dynamics.

(*a*) *Secure chaos communications*

The idea to hide an information signal within a chaotic carrier stems from the demonstration of the synchronisation capability between two distant chaotic oscillators, provided a suitable coupling between the emitter and the receiver can be designed [35]. Indeed, when a waveform can be synchronised, this usually means it can be used as an information carrier. The most common carrier in classical communications systems is the sine waveform, for which a receiver typically performs frequency synchronisation in order to achieve the demodulation of the carried information. Replacing the sine waveform by a broadband noise-like chaotic waveform does change the concept of information transmission via a carrier signal, as long as synchronisation of the chaotic carrier is possible. Such a synchronisation capability for chaotic signal, was orignally thought to be impossible because of the well known sensitivity to initial conditions of chaotic dynamics. Chaos synchronisation is thus the triggering scientific result for the field of chaos communications. A rough explanation for the synchronisation requirement in chaos communications, can be given as follows (we refer the reader to the prolific literature on chaos synchronization for more details, see e.g. [5]). The transmitted signal, which is available for anyone listening to the public transmission channel, is the result of the clear information signal superimposed onto the large amplitude chaotic carrier. Recovery of the masked information into the chaotic carrier, can be achieved if one is able at the decoder side to replicate the same chaotic carrier waveform (usually called identical synchronisation). In an authorised decoder, the locally synchronised chaotic carrier is subtracted from the received signal to result in the recovery of the original information (see the middle plots in Fig.4, upper: masked signal, chaos plus information; lower: unmasked information). Chaos, as a broadband signal much more complex than a sine waveform, offers the possibility to protect the transmitted information via the masking, and via the difficulty for achieving a successfull synchronisation. Indeed, synchonisation usually requires the knowledge of numerous physical parameters defined at the emitter for the generation of the chaotic carrier. These physical parameters and their precise setting at the emitter, usually form the secret key required also at the receiver for a proper decoding via chaos synchronisation.

Electro-optic delay dynamics offered in that context several attractive advantages: they increased dramatically the phase space dimension compared to the first experimental demonstration. The first demonstrations were indeed making use of electronic circuits generating chaotic carrier in a 3D phase space only [12], with easily recognisable spectra. On the contrary, the chaotic solutions of highly nonlinear delay dynamics exhibit a nearly flat and broadband Fourier spectrum, and a nearly Gaussian probability density function. They are thus ressembling any white noise source, and they make much more challenging the identification of the secret key parameters. The use of an optical architectures also provided access to standard optical telecommunication bandwidth, due to the use of off-the-shell telecom optoelectronic, electronic, and electro-optic devices designed for more than 10 Gb/s optical data transmissions. The single loop oscillating scheme also allowed to implement unconditionnally stable chaos synchronisation

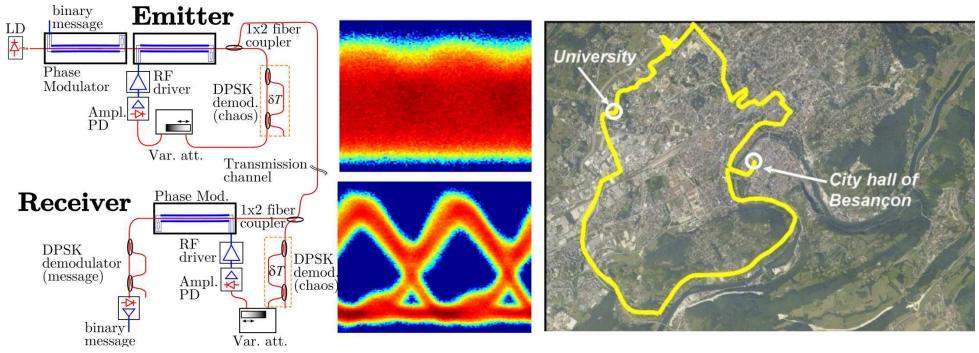

Figure 4. Electro-optic phase chaos communications: left: schematic of the emitter and receiver setup; middle: 10 Gb/s eye diagrams for the chaos encrypted signal (up) and recovered bit stream (low); right: satellite view of the "Lumière brothers" network in Besançon, where the first 10 Gb/s field experiment was performed. The Lumière brothers are the inventors of cinema, they were born in the city of Besançon.

configuration. Recently, experimental investigations of chaos communications succesfully achieved field experiment demonstration over installed fiber optic network, at more than 10 Gb/s data transmission. A specifically design EO setup was able to generate a chaotic optical phase used to carry the digital data with a DPSK encoding [25]. The demonstration was first performed on the small ring network in our city of Besançon, the so-called "Lumière" brothers ring network (see Fig.4). Further experiments over larger networks showed that our lab emitter-receiver setup can be plugged on an installed network, being operational over more than 100 km transmission link. The link quality of the encrypted transmission was found to be reasonnably good, with a net bit error rate at last of 10^{-7}. Such performance can be easily improved to error free transmission with standard digital error correction encoding.

(*b*) *Microwave optoelectronic oscillators*

The limit cycle solution of delay dynamics might offer also very attractive high performance features for another engineering applications. This concerns the generation of microwave oscillations at ultra high spectral purity level, e.g. for Radar sources. The actually oscillating microwave frequency F is roughly determined as $\omega_0/(2\pi)$ if we adopt the model in Eq.(2.3) for which the bandpass filter is highly selective, i.e. with $m \ll 1$. The long fiber delay line is here used to provide a long (compared to the oscillating period) energy storage element, which is typically required when high spectral purity is expected. In usual oscillators, this energy storage function is typically performed by resonators with very high quality factors. Quarz resonators are very well mature devices for achieving extreme stability via piezoelectric effects coupling electrical and mechanical vibrations. However, their Fourier frequency range, when very high stability is concerned, is currently limited up 100 MHz. In the microwave range, surface acoustic wave devices are making impressive progress, but photonic technologies are offering for the moment the most efficient solutions, e.g. through so-called optoelectronic oscillators (OEO). A basic, but very attractive feature is moreover that on the

contrary to oscillators based on electro-mechanical resonators, their quality factor is increasing with the operating frequency. This is easily explained due to the energy storage principle based on the delay of a microwave signal carried by an optical light beam: at a given linear loss coefficient (very low for fibers, typ. 0.2 dB/km), the $1/e$ attenuation is corresponding to a fixed fiber length L or delay τ_D, independently of the microwave modulation of the light carrier. Quality factor can then be defined as the number of open loop oscillating periods before their amplitude decay at $1/e$. Consequently, this quality factor scales linearly with the microwave frequency F, i.e. $Q = (n.L/c)\,F = \tau_D\,F$. Such a scaling is moreover valid in principle up to very high frequencies, due to the huge bandwidth of Telecom grade 1.5 μm monomode silica fibers. Practical limitations do not involved the ultra low loss feature, but other restricting physical phenomena at the origine of time delay fluctuations. This comprises for example refractive index variation due to temperature drifts, or laser phase noise transfer onto the microwave due to fiber dispersion. These limitations are currently imposing in practical OEO, a fiber length limit ca. of a few km (thus a few 10s of μs), thus shorter than to the $1/e$ attenuation limit. Figure 5 represents a typical phase noise spectrum recorded around an OEO with a central frequency $F = 10$ GHz. It was designed with an accurately thermalized 4 km fiber delay line, and a 50 MHz bandwidth "selective" electronic feedback filter. The zoom inset is a high resolution measurement of the width and height of the first side noise delay mode. This peak occurs at 50 kHz$= \tau_D^{-1}$ from the central oscillating mode. One can notice the extremely thin width (ca. 40 mHz) and the extreme height (110 dB, from the floor level at -140, to the top level accurately measured in the inset at -30), which are typical signatures of the large delay character of such an OEO.

From the more theoretical and nonlinear dynamics point of view, such extreme

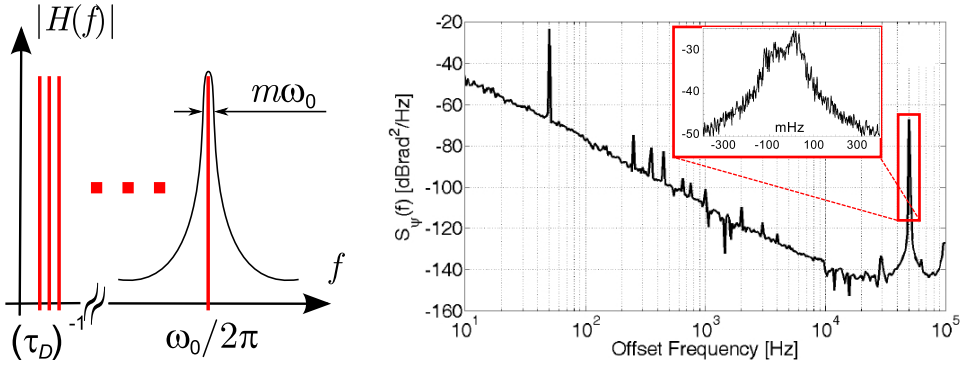

Figure 5. Microwave optoelectronic oscillator. Left: filter features relative to the delay mode in the Fourier domain. Right: Phase noise spectrum measurement around the central frequency at $\omega_0/2\pi = 10$ GHz; inset: spectral features (extremely thin and strong) of the first noisy side band delay mode[9] (the peak at 50 Hz is only a parasitic peak due to unavoidable electrical power line electro-magnetic pollution).

parameter conditions have brought also very interesting investigations. Indeed, with respect to the model given in Eqs. (2.2) and (2.3), one has a resonant filtering feedback corresponding to a very low damping $m \simeq 10^{-3} \ll 1$. This is in strong

contrast compared to the very high damping of the previous section a where $m \simeq 10^5 \gg 1$. However, though the feedback bandwidth is strongly reduced, the potential complexity or the number of degrees of freedom, is not necessarily very low, because the decrease of bandwidth is here compensated by the increase of the time delay. The relatively short delay in the previous section was about 10s of ns, it is here extended to several 10s of μs. The fondamental Fourier delay mode is now corresponding to a much lower frequency (typ. 50 kHz vs. 10 MHz for chaos communications), and the delay modes are becoming much more dense in the Fourier space. Though narrow bandpass feedback filter is involved around 10 GHz, the density of delay modes still allows for many tens to hundreds of these modes to be potantially involved in the dynamics. The narrow filter width of a few 10s of MHz feeds back potentially many of the 50 kHz-spaced delay modes. Highly complex delay dynamics can be expected, and was found to lead to other bifurcation scenarii when the feedback gain is increased: e.g. a Neimark-Sacker bifurcation occurs from the ω_0-Hopf limit cycle, leading to a torus characterized by a τ_D-periodic envelope modulation of the ω_0 microwave oscillation [8].

(*c*) *Photonic nonlinear transient computing*

The stable steady state is a solution of "a priori" relatively poor interest. And indeed, if one considers a fixed point, only a very low complexity level is obtained. The stable fixed point is however not a unique feature of the dynamical system it is generated from. One might at least associate to it the corresponding basin of attraction. Depending on the dynamics structure and dimension, the stable fixed point can become much more attractive in terms of related complexity. One could then not only analyze the local structure of a fixed point, but also its entire basin of attraction, as soon as a complex external signal can be designed to address in principle any possible trajectory driving to the fixed point: this is precisely what is used in an emerging application, "Reservoir Computing", which is making use of nonlinear transients complexity to perform computation. "Nonlinear Transient Computing" was also suggested in [11] and [31] as a naming which might refer more to the physics and nonlinear dynamics viewpoint. This novel computational principle was originally proposed independently in the early 2000 by the computer science / neural network computing community [18], and the brain cognitive research community [30]. It was initially referred to as Echo State Network, and Liquid State Machine, respectively. More recently, the unified name of "Reservoir Computing" [39] was proposed. The concept is closely inspired and related to the standard neural network computing, as represented in Fig.6. One of the main difference is to assume that the internal structure of the network does not need to be optimized during the learning phase. This internal structure typically only needs to be once randomly defined, via a connectivity matrix W^{I}. This is imposing a fixed, but still complex, dynamics for the global neural network. The learning phase then aims only at finding a suitable so-called "Read-Out" output via a Read-Out matrix W^{R}. The Read-Out consists simply in finding a hyperplane in the phase space of the network dynamics, from which the correct answer can be easily deduced. This Read-Out output consists of a linear combination of some of the network nodes that are animated by the complex transient motion, consecutivey to the injection into the network of the information to be processed. A suitable formatting of the input information is required, which is practically

defined by an input layer connection to the nodes of the network. This introduces a data connectivity matrix W^{D}, i.e. the way the input information is injected into the complex phase space. One of the most important advantage compared to classical neural network computing, resides in the fact that the learning is strongly simplified. It is usually performed successfully via an always existing solution of a simple ridge regression. This regression results in the calculation of W^{R}. Despite its much lower algorithmic complexity which is essentially reduced to the learning procedure, this approach already showed very good results on various complex tasks. Moreover, performances at the level of the most efficient classical neural network approaches have been achieved, and sometimes they are even outperforming them[19].

Very recently, in the frame of the European project PHOCUS, this novel

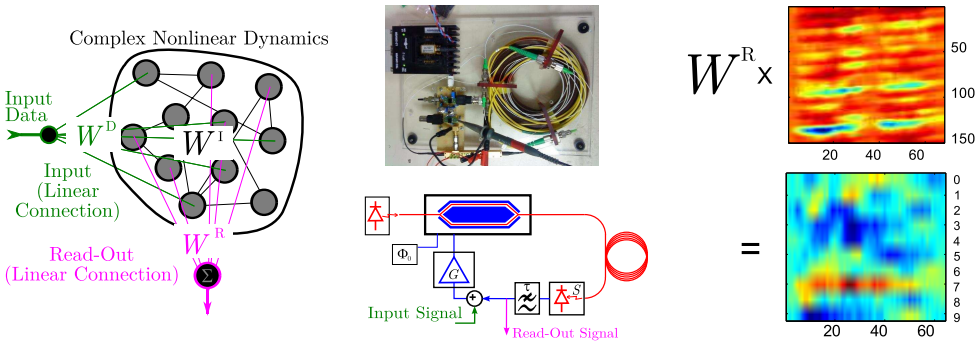

Figure 6. Photonic Nonlinear Transient Computing, or Reservoir Computing, with electro-optic delay dynamics. Left: general architecture of neural network computing. Middle: picture of the EO setup, and schematic of the setup similar to Fig.1. Right: experimental result with an already learnt Read Out matrix W^{R}, multiplied by the 2D pattern representing the transient response of the delay dynamics. The horizontal axis represents the discrete time index k labelling the time delay interval over the processing duration. The vertical axis represents the node index n (from 1 to 150), labelling the sampled amplitudes within each of the successive time delay intervals. The transient is generated by an external signal corresponding to the input information, here an acoustic speech (spoken digit) to be recognised. The matrix product gives a Read Out output where digit 7 can be easily identified as the most red-colored line among the 10 possible digits (0 to 9).

computational approach was addressed from the experimental point of view, with the use of a delay dynamics instead of a network of nodes. A first approach was tested with an electronic Mackey-Glass delay dynamics [1]. This first electronic demonstration was then also extended to a photonic design [24, 34, 31] directly inspired by the setup in Fig.1. These successful implementations of Reservoir Computing with delay dynamics, can be explained by a known analogy between infinite dimensional delay dynamics, and spatio-temporal dynamics [2] (see Fig.7). Standard neural network computer are usually materialized as a network of interconnected nodes, such as network of neurons, thus forming a complex spatio-temporal dynamics. This dynamical analogy between spatio-temporal dynamics and delay dynamics, allows a priori for the use of a delay dynamics for Reservoir Computing, in the place of the common spatially extended networks. This analogy consists in a representation of a delay dynamics, as a virtual continuous-space and

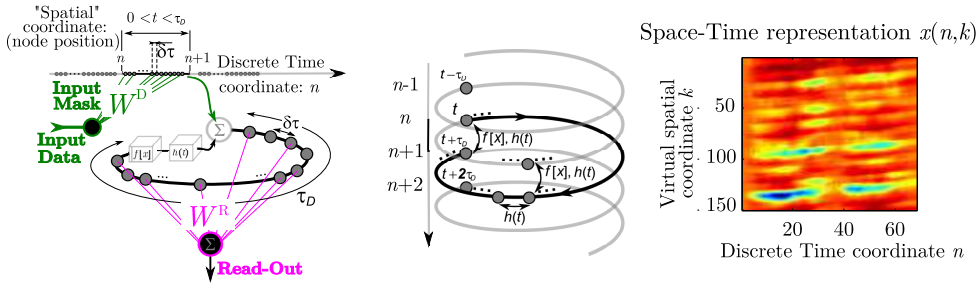

Figure 7. Graphical interpretation of the space-time analogy for a delay dynamical system used as a Nonlinear Transient Computer. Left: the input data are multiplexed in time through the use of a mask. Time multiplexing plays the role of addressing the virtual spatial nodes with the input data, with different weights. The virtual spatial nodes are "fine" temporal positions within a time delay of the nonlinear delayed feedback dynamics. They are separated by the quantity $\delta\tau$. The same nodes are used to perform the Read-Out, as a linear combination of these node amplitudes during the transient response of the delay dynamics. Middle: the delay dynamics is interpreted in terms of nodes interconnections. The impulse response $h(t)$ provides a short term connectivity, or equivalently a short distance spatial connectivity between the nodes. The nonlinear delayed term appears as a long term connectivity, or a temporal update from one time delay to the next, for each node. Right: spatio-temporal graph of a nonlinear delay dynamical transient. The fine temporal structure is the virtual spatial coordinate represented vertically. The time step from one time delay to the next, represents the discrete time iteration.

discrete-time dynamics. The discrete-time motion is corresponding to a round trip in the delay oscillation loop, indexed by an integer k labelling the number of the current τ_D-interval. The virtual continuous-space consists of the fine temporal motion of the dynamics, of the order of τ, and occuring within one "coarse" time delay interval. The nodes of the virtual network are then defined as N temporal positions within a time delay. Each node $x_n(k)|n \in [1, N]$ has a discrete time motion from one delay interval to the next, as k is increased to $k+1$. The 2D pattern $x(n, k)$ forms a representation of the transient motion, on which one has to apply the Read-Out matrix W^{R} in order to find the expected answer (see Fig.6). Experiments based on nonlinear delay dynamics used as the virtual complex dynamical network involved in a nonlinear transient computer, have been successfully conducted on benchmark tests such as spoken digit recognition, time series prediction and nonlinear channel equalization. Moreover, the achieved performances in these real-world physical setups are very close to the ones obtained from pure numerical simulations, opening very interesting perspectives on many practical problems that can not be solved easily and/or fast enough with standard digital computers.

4. Conclusions and future issues

Electro-optic delay dynamical systems have triggered during the last 15 years an important scientific activity, nicely balanced and cross-fertilized between fundamental issues and novel applications. It took benefit from the intrinsic complexity and dimensionality of the numerous and various possible dynamics.

Powerful applications have been at the origine of specific dynamical features due to setup modifications guided by applications. These specific dynamical features have been then also explored from the theoretical point of view. Examples in this review have covered applications concerned by three solutions of delay equations, from high dimensional chaos to the complex transients leading to a stable fixed point, through the extreme regularity of a limit cycle solution. A typical illustration of the cross-fertilisation can be the following one: broadband chaos was used in the frame of secure optical communication, which could only be designed with bandpass optoelectronic feedback, thus resulting in an integral term in the modeling equation. This term was then found to be at the origine of whether new periodic regimes, or stable ones which were known to be unstable or metastable. A important horizon is still open in this framework, and many issues remain to be addressed, again both from the application point of view and from the theoretical one. The nonlinear interactions between the limit cycle features, and the phase noise performance in microwave OEO, requires fundamental investigations of noisy delay equations. The phase space feature around the stable fixed point used for nonlinear transient computing needs to be deeper understood, especially from the information theory point of view, in order to optimize the processing power of this novel computational principle.
Last but not least, we anticipate that novel fundamental dynamical properties will appear again via novel design approaches for improved applications involving delay dynamical systems. A probably important technological evolution in delay dynamics, which already started in the case of external cavity lasers [4], concerns the use of integration possibilities and micro- nano-technologies for the realisation of delay dynamical systems. This also includes optical disk resonators currently investigated for broadband comb generation and extreme stability time-frequency systems. These setups have been clearly identified as involving both the delay in the ring, and also a distributed nonlinear light-matter interactions between the numerous cavity/delay modes [7].

Acknowledgment

Most of the results presented above were obtained in the framework of several projects and collaborations, in which L.L. has participated as a group leader of the FEMTO-ST institute. The many aspects of these results are thus definitely the consequence of numerous "highly constructive interferences" with many co-workers (colleagues, collaborators, PhD students). I first apologise for the ones who might be missing in the following list, but I ensure them also for my respectful recognition of their contribution. The main contributors can thus be found at least among the following persons: Jean-Pierre Goedgebuer, Jean-Marc Merolla, Maxime Jacquot, Yanne Chembo, John Dudley, Pierre Lacourt, Vladimir Udaltsov, Thomas Erneux, Pere Colet, Ingo Fischer, Claudio Mirasso, Jia-Ming Liu, Min Won Lee, Rajarshi Roy, Atsushi Uchida, Raymond Quéré, Luis Pesquera, Pierre Glorieux, Yves Pomeau, Maxi San Miguel, Daniel Gauthier, Lucas Illing, Dimitris Syvridis, Apostolos Argyris, Alan Shore, Valerio Annovazzi-Lodi, etc.... This work was also more recently essentially supported by the European PHOCUS project (FP7-2009-ICT-240763) and by the Labex ACTION program (contract ANR-11-LABX-01-01). L.L. also thanks the support of the *Institut universitaire de France* for the efficient and

highly appreciated research conditions it offered him during the last 5 years, as a Junior member of this institution.

References

[1] L. Appeltant, M. C. Soriano, G. Van der Sande, J. Danckaert, S. Massar, J. Dambre, B. Schrauwen, C. R. Mirasso, and I. Fischer. Information processing using a single dynamical node as complex system. *Nature Commun.(London)*, 2(468):1–6, September 2011.

[2] F. T. Arecchi, G. Giacomelli, A Lapucci, and R. Meucci. Two–dimensional representation of a delayed dynamical system. *Phys. Rev. A*, 45(7):R4225–R4228, April 1993.

[3] A. Argyris, D. Syvridis, L. Larger, V. Annovazzi-Lodi, P. Colet, I. Fischer, J. G.arcia-Ojalvo, C. R. Mirasso, L. Pesquera, and A. K. Shore. Chaos–based communications at high bit rates using commercial fiber–optic links. *Nature (London)*, 438:343–346, November 2005.

[4] M. Argyris, A. M. Hamacher, K.E. Chlouverakis, A. Bogris, and D. Syvridis. Photonic integrated device for chaos applications in communications. *Phys. Rev. Lett.*, 100:194101, May 2008.

[5] S. Boccaletti, J. Kurths, G. Osipov, D.L. Valladares, C.S. Zhou. The synchronization of chaotic systems. *Physics Reports*, 366:1–101, January 2002.

[6] K.E. Callan, L. Illing, Z. Gao, D.J Gauthier, and E. Schöll. Broadband chaos generated by an optoelectronic oscillator. *Phys. Rev. Lett.*, 104:113901, March 2010.

[7] Y. K. Chembo and N. Yu. Modal expansion approach to optical-frequency-comb generation with monolithic whispering-gallery-mode resonators. *Phys. Rev. A*, 82:033801, September 2010.

[8] Y. K. Chembo, L. Larger, H. Tavernier, R. Bendoula, E. Rubiola, and P. Colet. Dynamic instabilities of microwaves generated with optoelectronic oscillators. *Opt. Lett.*, 32(17):2571–2573, September 2007.

[9] Y. K. Chembo, K. Volyanskiy, L. Larger, E. Rubiola, and P. Colet. Determination of phase noise spectra in optoelectronic microwave oscillators: A langevin approach. *IEEE J. Quantum Electron.*, 45(2):178–186, February 2009.

[10] A. B. Cohen, B. Ravoori, T. E. Murphy, and R. Roy. Using synchronization for prediction of high-dimensional chaotic dynamics. *Phys. Rev. Lett.*, 101:154102, October 2008.

[11] N. Crook. Nonlinear transient computation. *Neurocomputing*, 70:1167–1176, December 2007.

[12] K. M. Cuomo and A. V. Oppenheim. Circuit implementation of synchronized chaos with applications to communications. *Phys. Rev. Lett.*, 71(1):65–68, July 1993.

[13] H. M. Gibbs, F. A. Hopf, D. L. Kaplan, and R. L. Shoemaker. Observation of chaos in optical bistability. *Phys. Rev. Lett.*, 46(7):474–477, February 1981.

[14] J.-P. Goedgebuer, P. Levy, L. Larger, C.-C. Chen, and W. T. Rhodes. Optical communication with synchronized hyperchaos generated electrooptically. *IEEE J. Quantum Electron.*, 38(9):1178–1183, September 2002.

[15] K. Ikeda. Multiple-valued stationary state and its instability of the transmitted light by a ring cavity system. *Optics Commun.*, 30(3):257–261, August 1979.

[16] K. Ikeda, K. Kondo, and O. Akimoto. Successive higher harmonic bifurcations in systems with delayed feedback. *Phys. Rev. Lett.*, 49(20):1467–1470, November 1982.

[17] L. Illing and D.J. Gauthier. Hopf bifurcations in time–delay systems with band–limited feedback. *Physica D*, 210:180–202, August 2005.

[18] H. Jaeger. The "echo state" approach to analysing and training recurrent neural networks. *GMD Report*, 148, 2001.

[19] H. Jaeger and H. Haas. Harnessing nonlinearity: predicting chaotic systems and saving energy in wireless communication. *Science*, 304:78–80, April 2004.

[20] Y. C.Kouomou, P. Colet, L. Larger, and N. Gastaud. Chaotic Breathers in Delayed Electro-Optical Systems. *Phys. Rev. Lett.*, 95:203903, 2005.

[21] L. Larger, J.-P. Goedgebuer, and J.-M. Merolla. Chaotic oscillator in wavelength: A new setup for investigating differential difference equations describing nonlinear dynamics. *IEEE J. Quantum Electron.*, 34(4):594–601, April 1998.

[22] L. Larger, J.-P. Goedegbuer, and V. S. Udalsov. Ikeda–based nonlinear delayed dynamics for application to secure optical transmission systems using chaos. *C.R. de Physique 4*, 5(6):669–681, July 2004.

[23] L. Larger, P.-A. Lacourt, S. Poinsot, and M. Hanna. From flow to map in an experimental high-dimensional electro-optic nonlinear delay oscillator. *Phys. Rev. Lett.*, 95:043903, July 2005.

[24] L. Larger, M. C. Soriano, D. Brunner, L. Appeltant, J. M. Gutierrez, L. Pesquera, C. R. Mirasso, and I. Fischer. Photonic information processing beyond turing: an optoelectronic implementation of reservoir computing. *Opt. Express*, 20(3):3241–3249, January 2012.

[25] R. Lavrov, M. Jacquot, and L. Larger. Nonlocal nonlinear electro-optic phase dynamics demonstrating 10 gb/s chaos communications. *IEEE J. Quantum Electron.*, 46(10):1430–1435, October 2010.

[26] R. Lavrov, M. Peil, M. Jacquot, L. Larger, V. S. Udaltsov, and J. M. Dudley. Electro–optic delay oscillator with non–local non linearity: optical phase dynamics, chaos, and synchronization. *Phys. Rev. E*, 80:026207, August 2009.

[27] M. Le Berre, É. Ressayre, A. Tallet, and H. M. Gibbs. High–dimension chaotic attractors of a nonlinear ring cavity. *Phys. Rev. Lett.*, 56(4):274–275, January 1986.

[28] M. Le Berre, É. Ressayre, A. Tallet, H. M. Gibbs, D. M. Kaplan, and M. H. Rose. Conjecture on the dimension of chaotic attractors of delayed–feedback dynamical systems. *Phys. Rev. A*, 35(9):4020–4022, May 1987.

[29] M. W. Lee, L. Larger, V.S. Udaltsov, É. Genin, and J.-P. Goedgebuer. Demonstration of a chaos generator with two time delays. *Opt. Lett.*, 29(4):325–327, February 2004.

[30] W. Maass, T. Natschläger, and H. Markram. Real–time computing without stable states: A new framework for neural computation based on perturbations. *Neural Computation*, 14(11):2531–2560, 2002.

[31] R. Martinenghi, S. Rybalko, M. Jacquot, Yanne Kouomou Chembo, and Laurent Larger. Photonic nonlinear transient computing with multiple-delay wavelength dynamics. *Phys. Rev. Lett.*, 108:244101, January 2012.

[32] T. E. Murphy, A. B. Cohen, B. Ravoori, K. R. B. Schmitt, A. V. Setty, F. Sorrentino, C. R. S. Williams, E. Ott, and R. Roy. Complex dynamics and synchronization of delayed-feedback nonlinear oscillators. *Phil. Trans. R. Soc. A*, 368:343–366, 2010.

[33] A. Neyer and E. Voges. Dynamics of electrooptic bistable devices with delayed feedback. *IEEE J. Quantum Electron.*, 18(12):2009–2015, December 1982.

[34] Y. Paquot, F. Duport, A. Smerieri, J. Dambre, B. Schrauwen, M. Haelterman, and S. Massar. Optoelectronic reservoir computing. *Scientific Reports*, 2:287, February 2012.

[35] L. M. Pecora and T. L. Carroll. Synchronization in chaotic systems. *Phys. Rev. Lett.*, 64(8):821–824, November 1990.

[36] M. Peil, M. Jacquot, Y. C. Kouomou, L. Larger, and T. Erneux. Routes to chaos and multiple time scale dynamics in broadband bandpass nonlinear delay electro-optic oscillators. *Phys. Rev. E*, 79:026208, February 2009.

[37] B. Ravoori, A. B. Cohen, A. V. Setty, F. Sorrentino, T. E. Murphy, E. Ott, and R. Roy. Adaptive synchronization of coupled chaotic oscillators. *Phys. Rev. E*, 80:056205, November 2009.

[38] B. Ravoori, A. B. Cohen, J. Sun, A. E. Motter, T. E. Murphy, and R. Roy. Robustness of optimal synchronization in real networks. *Phys. Rev. Lett.*, 107:034102, July 2011.

[39] D. Verstraeten, B. Schrauwen, M. D'Haene, and D. Stroobandt. An experimental unification of reservoir computing methods. *Neural Networks.*, 2007.

[40] L. Weicker, T. Erneux, O. D'Huys, J. Danckaert, M. Jacquot, Y. Chembo, and L. Larger. Slow-fast dynamics for time-delay problems: theory and experiments. *Phyl. Trans. Roy. Soc. A*, 2012.

[41] L. Weicker, T. Erneux, O. D'Huys, J. Danckaert, M. Jacquot, Y. Chembo, and L. Larger. Strongly asymmetric square-waves in a time delayed system. *submitted*, 2012.

[42] L. Weicker, T. Erneux, M. Jacquot, Y. Chembo, and L. Larger. Crenelated fast oscillatory outputs of a two-delay electro-optic oscillator. *Phys. Rev. E*, 85:026206, February 2012.

[43] X. S. Yao and L. Maleki. High frequency optical subcarrier generator. *Electron. Lett.*, 30(18):1525–1526, September 1994.